Wideband Characterization of Urban Propagation Channels Using TD-UTD

Kleber L. Borges and Fernando J. S. Moreira
Universidade Federal de Minas Gerais, Depto. de Engenharia Eletrônica
Av. Pres. Antônio Carlos 6627, Pampulha, Belo Horizonte, MG, CEP 31270-901

***Abstract*— This work deals with the application of the Time Domain Uniform Theory of Diffraction (TD-UTD) in wideband propagation predictions for urban scenarios. Results are presented and compared against those obtained by the application of an inverse Fourier transform upon the usual frequency-domain UTD and method of moments (MoM). In the frequency domain, multiple diffractions and lossy obstacles can be accounted for. However, in the adopted TD-UTD formulation only a single diffraction and perfect electric or magnetic conductors are considered. For the present TD-UTD analysis and for a typical urban radio channel where the antennas' heights are small compared to the buildings' heights, it is shown that the consideration of ground as a perfect magnetic conductor instead of an electric one provides a better approach for a vertical polarization over lossy ground. The buildings are treated as perfect electric conductors.**

***Index Terms*— Urban propagation channel, ultra wideband, time domain uniform theory of diffraction.**

I. Introduction

Recently, technologies based on ultra wideband (UWB) transmission are being developed, like impulse radio and high resolution radars. According to the U.S. Federal Communications Commission (FCC), UWB signals are those with a bandwidth greater than 25% of the central frequency, measured from the 10dB attenuation points, or greater than 1.5 GHz [1]. In principle, it is more convenient to analyze such systems directly in the time domain, as they are generally based on the transmission of many consecutive pulses and the representation of a pulse in time domain is simpler than in frequency domain.

To obtain the radio channel response due to a pulse excitation, two techniques can be used. One is to calculate the channel response for a lot of discrete frequencies and then apply an inverse fast Fourier transform (IFFT) to establish the time response. Another is to perform the analysis directly in time domain. Being N_f number of discrete frequencies, it is known that the IFFT requires $N_f \log_2 N_f$ operations whenever N_f is a power of 2 and N_f^2 otherwise [2]. Consequently, the shorter the pulse is, the greater will be the number of frequencies to be analyzed. In the time domain, however, the analysis requires just N_f instants of time for the same time window. Another problem that arises from the IFFT operation is aliasing. To avoid this problem, it is necessary the use of larger time windows and, consequently, larger N_f values, increasing the computational burden. In time domain this problem does not occur, and the time window may only have the desired instants of time. So, for the appropriate wideband characterization of radio channels, it is more convenient to adopt a time domain formulation whenever possible.

Fernando J. S. Moreira, fernando@eee.ufmg.br. This work was partially supported by CAPES and CNPq.

II. TD-UTD Impulse Response

Here, the radio channel will be approximated as a linear system, in which case its characterization is evaluated with the helpof its transfer function (or impulse response). In electromagnetic problems where space and time variations must be considered, this response is known as the time-domain Green's function, which is obtained from the environment response to a time-impulse source in a given location and with a proper polarization. Afterwards, the time response to more realistic signals is evaluated from its convolution with the associated Green's function as [3]

$$f(t) * g(t) = \int_{-\infty}^{\infty} f(\tau)\, g(t-\tau)\, \mathrm{d}\tau\,, \tag{1}$$

where $g(t)$ and $f(t)$ represent the Green's function and a Maxwellian excitation of any kind, respectively.

To obtain the radio channel impulse response, it is used a combination of ray-tracing, Time Domain Geometric Optics (TD-GO) and TD-UTD. The TD-GO and TD-UTD expressions are obtained from the application of the Analytic Time Transform (ATT) in the well known frequency domain GO and UTD expressions for perfect conductors [4]. The TD-GO and TD-UTD expressions are valid near the arriving time of the ray [4].

A. ATT and some useful properties

The ATT is defined as [4]

$$\overset{+}{f}(t) = \frac{1}{\pi} \int_{-\infty}^{\infty} F(\omega)\, u(\omega)\, e^{j\omega t}\, \mathrm{d}\omega, \quad \text{for } \mathrm{Im}\,(t) > 0, \tag{2}$$

where ω is the angular frequency, $F(\omega)$ is the Fourier transform of $f(t)$ given by

$$F(\omega) = \int_{-\infty}^{\infty} f(t)\, e^{-j\omega t}\, \mathrm{d}t\,, \tag{3}$$

and $u(\omega)$ is the Heaviside step, given by

$$u(\omega) = \begin{cases} 0 & \omega < 0 \\ 1/2 & \omega = 0 \\ 1 & \omega > 0 \end{cases} . \tag{4}$$

The "+" sign over f means an analytical signal in a complex-time domain. As no radiation occurs for $\omega = 0$, the ATT can be rewritten as [4]

$$\overset{+}{f}(t) = \frac{1}{\pi} \int_0^\infty F(\omega)\, e^{j\omega t}\, \mathrm{d}\omega\,, \quad \text{for } \mathrm{Im}\,(t) > 0. \tag{5}$$

The relation between $\overset{+}{f}(t)$ and the desired real function $f(t)$ is given by [4]

$$\overset{+}{f}(t) = f(t) + j\,\mathcal{H}[f(t)]\,, \quad \text{for } \mathrm{Im}\,(t) = 0\,, \tag{6}$$

where $\mathcal{H}[f(t)]$ the Hilbert transform of $f(t)$. Consequently,

$$f(t) = \mathrm{Re}\left[\overset{+}{f}(t)\right], \quad \text{for } \mathrm{Im}\,(t) = 0. \tag{7}$$

It is important to observe from (5) the close relation between the ATT and the inverse Fourier transform, which eneables the use of several properties of the Laplace and Fourier transforms [4].

B. TD-GO electromagnetic fields

In this work the environment is assumed linear, isotropic, homogeneous and non-dispersive (i.e., the atmosphere is the vacuum and any obstacle will be assumed a perfect conductor). Recalling the phasor representation in the frequency domain and that the UTD is an asymptotic theory, the time-harmonic radiation is represented by ray fields and only the transmitter gain and the phase of the field will vary with the frequency. The gain variation will be discussed afterwards, when the time dependance of the source is modeled. The phase variation, under the present circumstances, will be always of the form $\exp[-j(\omega/c)s]$, where c is the light velocity and s represents the distance along the ray path. So, from (5), the phase term is transformed by the ATT into the analitic delta function $\overset{+}{\delta}(t - s/c)$, given by [4]

$$\overset{+}{\delta}(t) = \begin{cases} j/(\pi t)\,, & \mathrm{Im}\,(t) > 0 \\ \delta(t) + \mathrm{pv}[j/(\pi t)]\,, & \mathrm{Im}\,(t) = 0 \end{cases} , \tag{8}$$

where $\mathrm{pv}(\cdot)$ stands for the Cauchy principal value.

So, applying the ATT to the usual GO expressions [5], the impulse response for a TD-GO field is simply given by [4]

$$\overset{+}{\vec{e}}_I(s,t) = j^m\, |A(s)|\ \overset{+}{\delta}(t - s/c)\, \hat{p}\,, \tag{9}$$

where $A(s)$ is the usual GO attenuation factor, $\hat{p}$ represents the electric field polarization, and m is the number of line or smooth caustics that the ray has to transverse in the forward direction (i.e., for $s > 0$). In practical terms, m is the number of negative radii of curvature of the wavefront at $s = 0$ and may be equal to 0, 1, or 2. For example, for radiation from line or point sources, $m = 0$. Consequently, the term j^m accounts for the Gouy phase shift. The reason for stressing it in (9) is to simplify the manipulation of the real and imaginary parts of the analytical signal, before the application of (7). Finally, the index I in (9) stresses that this analytic field is to be interpreted as one of the many multipath components in a radio channel.

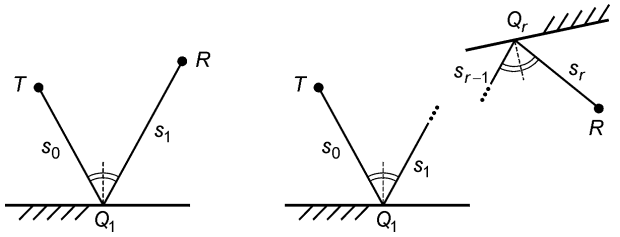

(a) (b)

Fig. 1. (a) Single and (b) multiple reflections optical paths.

C. Reflected fields

The treatment of reflections by the TD-GO is quite direct if one assumes a perfectly conducting surface. Let's assume the geometry depicted by Fig. 1(a). In the frequency domain, the phasor representation of the reflected field at the receiver (R) is given by [5]

$$\vec{E}(R) = \bar{\mathbf{R}}_\mathbf{1} \cdot \vec{E}(Q_1)\, j^{m_1}\, |A(s_1)|\, e^{-jks_1}\,, \tag{10}$$

where $k = \omega/c$, $\bar{\mathbf{R}}_\mathbf{1}$ is the dyadic reflection coeficient for the problem at hand, given in terms of the Fresnel reflection coeficients, m_1 is the number of negative radii of curvature of the reflected wavefront just after Q_1, and $\vec{E}(Q_1)$ is the incident field just before Q_1, whose ray-field representation may be represented as

$$\vec{E}(Q_1) = E_o\, j^{m_0}\, |A(s_0)|\, e^{-jks_0}\, \hat{p}\,, \tag{11}$$

where m_0 is defined as usual, now for the incident wavefront, and E_o is an arbitrary amplitude, assumed constant for the time being.

It is important to observe that for lossless surfaces, the reflection dyad does not vary with ω and, consequently, will not be affected by the ATT. For instance, for perfect conductors the Fresnel reflection coeficientes are equal to ± 1, with the sign depending on the wave polarization and on the conductor being a perfectly electric or magnetic. So, substituting (11) into (10) and applying (5) afterwards, the analytical representation of the reflected field is given by [4]

$$\overset{+}{\vec{e}}_I(R,t) = E_o\, j^{(m_0+m_1)} |A(s_0)A(s_1)|\, \bar{\mathbf{R}}_\mathbf{1} \cdot \hat{p}\ \overset{+}{\delta}\left(t - \frac{s_0 + s_1}{c}\right). \tag{12}$$

For multiple reflections, like in Fig. 1(b), the result is quite obvious:

$$\overset{+}{\vec{e}}_I(R,t) = E_o\, j^{M_T}\, |A_T|\, \vec{R}_T\ \overset{+}{\delta}\left(t - \frac{S_T}{c}\right), \tag{13}$$

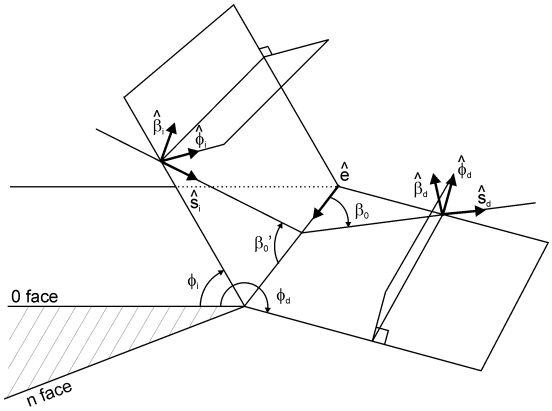

Fig. 2. Edge fixed coordinate system.

where

$$\vec{R}_T = \bar{\mathbf{R}}_{\mathbf{r}} \cdot \bar{\mathbf{R}}_{\mathbf{r-1}} \cdot \ldots \cdot \bar{\mathbf{R}}_{\mathbf{2}} \cdot \bar{\mathbf{R}}_{\mathbf{1}} \cdot \hat{p}\,, \tag{14}$$

$$M_T = m_0 + m_1 + m_2 + \ldots + m_{r-1} + m_r\,, \tag{15}$$

$$A_T = A(s_0)A(s_1)A(s_2)\ldots A(s_{r-1})A(s_r)\,, \tag{16}$$

$$S_T = s_0 + s_1 + s_2 + \ldots + s_{r-1} + s_r\,. \tag{17}$$

From the previous equations it must be clear that, once the ray trajectories are obtained, the calculation of the field at the receiver is a simple task, as far as the reflection coeficients do not depend on ω. In the present work, the ray tracing algorithm is that of [6], based on the image theory and also accounting for ground reflection.

D. Time Domain Uniform Theory of Diffraction

The analytical impulse response for the field diffracted by a perfectly electric conducting (PEC) wedge was developed in [4] and only the final expressions are presented. Such formulation does not include slope diffraction. The geometrical parameters of interest are illustrated in Fig. 2. Assuming that the wedge is illuminated by an incident field with a phasor representation in the frequency domain like the one in (11), the analytical difracted field at an observation point R is given by [4]:

$$\overset{+}{\vec{e}}_I(R,t) = E_o\, j^{(m_0+m_d)}\, |A(s_0)A(s_d)|\ \overset{+}{\bar{\mathbf{D}}}\left(t - \frac{s_0+s_d}{c}\right)\cdot\hat{p}\,, \tag{18}$$

where s_d is the distance from the diffraction point (located at the wedge's edge) to R, $A(s_d)$ is the usual UTD attenuation factor (as it does not depend on ω for a PEC wedge) [5], $m_d = 0$ if the edge caustic distance is positive and 1 otherwise, and $\overset{+}{\bar{\mathbf{D}}}\ (\tau)$ is the dyadic diffraction coefficient given by

$$\overset{+}{\bar{\mathbf{D}}}(\tau) = \overset{+}{D}_s(\tau)\,\hat{\beta}_d\,\hat{\beta}_i + \overset{+}{D}_h(\tau)\,\hat{\phi}_d\,\hat{\phi}_i\,, \tag{19}$$

with the unit directions $\hat{\beta}_i$, $\hat{\beta}_d$, $\hat{\phi}_i$, and $\hat{\phi}_d$ defined as in Fig. 2. Note that here $\hat{\beta}_d$ and $\hat{\phi}_d$ are the opposite of those usually defined, for example, in [4] and [5]. The soft and hard analytical diffraction coefficients for the PEC wedge are given by [4]:

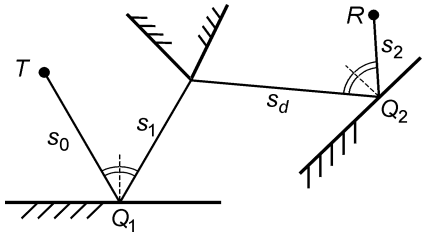

Fig. 3. Multiple reflections with a single diffraction.

$$\overset{+}{D}_{s,h}(\tau) = \overset{+}{D}_1(\tau) + \overset{+}{D}_2(\tau) \mp \overset{+}{D}_3(\tau) \mp \overset{+}{D}_4(\tau)\,, \tag{20}$$

where, for a wedge with flat faces,

$$\begin{aligned}
\overset{+}{D}_1(\tau) &= B_o\,\cot\left(\frac{\pi+\beta^-}{2n}\right)\ \overset{+}{F}(x_1,\tau)\,,\\
\overset{+}{D}_2(\tau) &= B_o\,\cot\left(\frac{\pi-\beta^-}{2n}\right)\ \overset{+}{F}(x_2,\tau)\,,\\
\overset{+}{D}_3(\tau) &= B_o\,\cot\left(\frac{\pi+\beta^+}{2n}\right)\ \overset{+}{F}(x_3,\tau)\,,\\
\overset{+}{D}_4(\tau) &= B_o\,\cot\left(\frac{\pi-\beta^+}{2n}\right)\ \overset{+}{F}(x_4,\tau)\,,
\end{aligned} \tag{21}$$

with

$$\begin{aligned}
B_o &= \frac{-1}{2n\sqrt{2\pi}\sin\beta_0}\,,\\
\overset{+}{F}(x,\tau) &= \frac{\sqrt{x/\pi}\,(j\sqrt{\tau}+\sqrt{x/c})}{\sqrt{\tau}\,(\tau+x/c)}\,,\\
x_1 &= L^i\,a^+(\beta^-)\,,\\
x_2 &= L^i\,a^-(\beta^-)\,,\\
x_3 &= L^{rn}\,a^+(\beta^+)\,,\\
x_4 &= L^{ro}\,a^-(\beta^+)\,,\\
\beta^+ &= \phi_d + \phi_i\,,\\
\beta^- &= \phi_d - \phi_i\,.
\end{aligned}$$

All the above parameters refer to the usual frequency domain UTD for PEC wedges and are explained in a comprehensive fashion in [5] and [4].

E. Multiple reflections with a single diffraction

Now let's consider the situation depicted in Fig. 3 where the PEC wedge's diffraction occurs between two reflections. In this situation, from the Dirac's delta property, togheter with (13) and (18), the analytic field at the receiver is given by

$$\begin{aligned}
\overset{+}{\vec{e}}_I(R,t) = E_o\, j^{(m_0+m_1+m_d+m_2)}\, &|A(s_0)A(s_1)A(s_d)A(s_2)|\\
&\times \bar{\mathbf{R}}_{\mathbf{2}}\cdot\overset{+}{\bar{\mathbf{D}}}\left(t - \frac{s_0+s_1+s_d+s_2}{c}\right)\cdot\bar{\mathbf{R}}_{\mathbf{1}}\cdot\hat{p}\,.
\end{aligned} \tag{22}$$

The exclusion or inclusion of other reflection mechanisms in (22) is quite direct for the present scenario.

F. Inclusion of a realistic antenna radiation

In practice, the antenna radiation characteristics change with ω and the field complex amplitude E_o must not be considered as a constant, specially for wideband applications. So, the actual multipath componente $\overset{+}{\vec{e}}_I(t)$ must be convoluted with $\overset{+}{e}_o(t)$, which is the ATT of $E_o(\omega)$. An efficient way to evaluate such convolution is presented in [4] and briefly discussed below. The technique is based on the expansion of $E_o(\omega)$ into a series of exponentials:

$$E_o(\omega) = \sum_{n=1}^{N} A_n e^{-\alpha_n \omega}, \qquad \text{for} \quad \omega > 0, \tag{23}$$

where N, A_n, and α_n are specified according to the antenna radiation characteristics. Applying (5) and (8), $\overset{+}{e}_o(t)$ is readly obtained [4]:

$$\overset{+}{e}_o(t) = \sum_{n=1}^{N} \frac{jA_n/\pi}{t + j\alpha_n} = \sum_{n=1}^{N} A_n \overset{+}{\delta}(t + j\alpha_n), \quad \text{for } \alpha_n > 0. \tag{24}$$

As $\overset{+}{e}_o(t)$ is represented as a series of analytical delta functions, the convolution becomes a simple task and, consequently, the multipath components presented in (9), (12), (13), (18), and (22), for the many possible multipath mechanisms considered in this work, should be substituted as follows:

$$\overset{+}{\vec{e}}_I(t) \longrightarrow \overset{+}{\vec{e}}_I(t) * \overset{+}{e}_o(t) = \sum_{n=1}^{N} A_n \overset{+}{\vec{e}}_I(t + j\alpha_n), \tag{25}$$

in which case (9), (12), (13), (18), and (22) are still extremely useful.

In the simulations to be presented, the adopted $E_o(\omega)$ is given by [4]

$$E_o(\omega) = C_o (1 - e^{-\omega T})^{P_1} e^{-\omega P_2 T}, \tag{26}$$

where

$$T = \frac{1}{2\pi f_c} \ln\left(\frac{P_1 + P_2}{P_2}\right), \tag{27}$$

f_c is the pulse central frequency, P_1 and P_2 are exponents used to control the shape of $E_o(\omega)$, and

$$C_o = \left(\frac{P_1 + P_2}{P_1}\right)^{P_1} \left(\frac{P_1 + P_2}{P_2}\right)^{P_2}. \tag{28}$$

Once the desired representation of $E_o(\omega)$ is established with the help of (26), than the parameters N, A_n, and α_n of (23) are readly obtained following the procedure presented in [4].

III. Numerical Results

The ray-tracing algorithm used in this work is based on multiple image theory for obtaining rays with a limited number of reflections. More details about this theory can be found in [6], [7].

First, it will be analyzed the case shown in Fig. 4, where the cylinder is an electric perfect conductor with 2 m side. The transmitter antenna is a current line and the receiver antenna is isotropic. The channel response will be analyzed for some values for the angle ϕ, in a circular path with 4 m radius. The excitation pulse have $f_c = 2$ GHz, $M = 1$ and $N = 2$. Its shape is shown in Fig. 5. It will be analyzed the results obtained from the UTD [8] and TD-UTD, and the reference will be the Method of Moments (MoM) [9]. In this work, the results of UTD and MoM after the IFFT operation will be labeled UTD-IFFT and MoM-IFFT, respectively. In ray-tracing algorithm, it will be considered rays until 2 diffractions for the UTD-IFFT and until 1 diffraction for the TD-UTD [6]. For the MoM, it will be used 5 segments for wavelength otherwise.

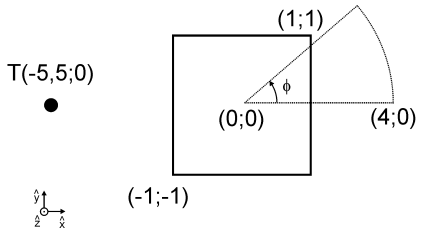

Fig. 4. Geometry to be analyzed. The environment is 2D and the transmitter antenna is a line current. The receiver antenna is isotropic. All dimensions are in meters.

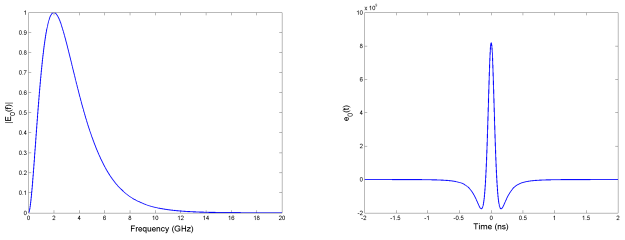

(a) Pulse spectrum. (b) Pulse in time.

Fig. 5. Excitation shape for $M = 1$, $N = 2$ and $f_c = 2$ GHz.

The results for $\phi = 90$ are shown in Fig 6. The results obtained from TD-UTD are equal the UTD-IFFT results, because the TD-UTD formulation is obtained from UTD without any approximation. For $\phi = 180$, there is a reflected pulse, and its arriving time is near the arriving time of diffracted rays in wedges $(-1\text{m},-1\text{m})$ and $(-1\text{m},1\text{m})$. The results for both polarizations agree with the results obtained from MoM-IFFT.

Now, it will be analyzed a real case according to Fig. 8 [10]. The *quasi*-3D model will be used for the ray-tracing, i.e., the reflections in plain ground are considered [6], [7]. The transmitter antenna is a infinitesimal electric dipole, vertically polarized, 8,5 m height and localized in (241m,263m). The receiver antenna R is isotropic, 3,65 m height and localized in (510m,270m). It will be considered here only the UTD-IFFT and TD-UTD results, where it will be analyzed the lossy effect in a typical urban scenario. The excitation used has $f_c = 5$ GHz, $M = 1$ and $N = 2$, which has a spatial dimension (approximately

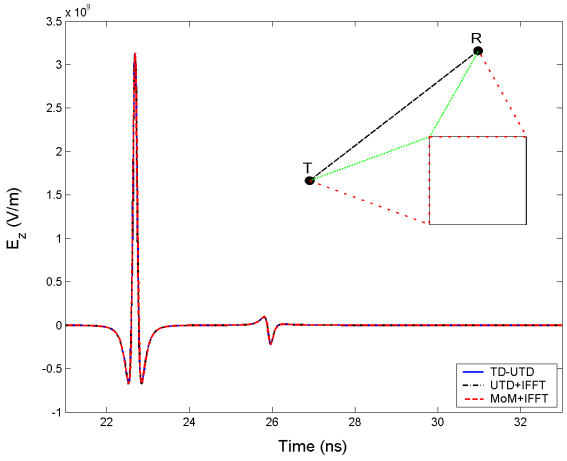

(a) TMz polarization

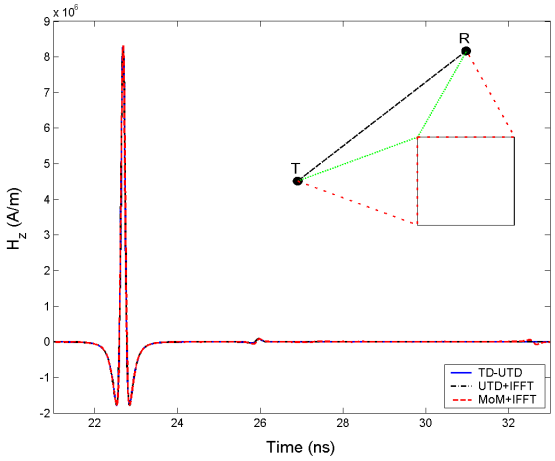

(b) TEz polarization

Fig. 6. Results for geometry of Fig 4 with $\phi = 90$. For MoM where used 5 seg/λ.

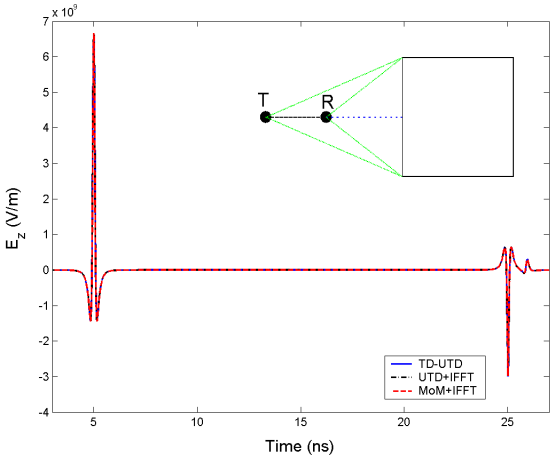

(a) TMz polarization

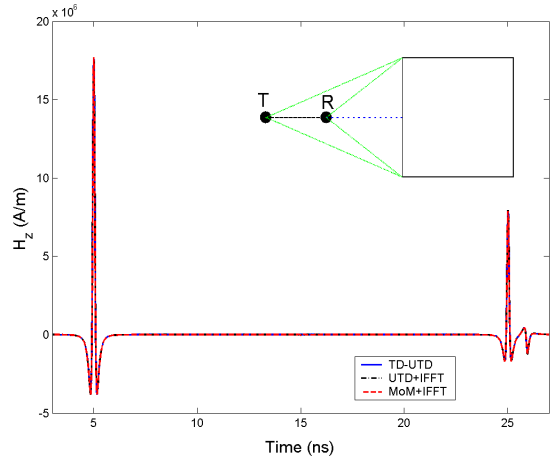

(b) TEz polarization

Fig. 7. Results for geometry of Fig 4 with $\phi = 180$. For MoM where used 5 seg/λ.

0,18 m) very less than the dimensions of obstacles into the environment. The pulse width is into characteristics for Time-Modulated UWB (TM-UWB) system, i.e., between 0.2 and 1 ns [1]. For UTD-IFFT prediction, it was considered $\epsilon_r = 7$ and $\sigma = 0.2$ S/m for obstacles and $\epsilon_r = 15$ and $\sigma = 0.05$ S/m for the ground. For ray-tracing algorithm, it was considered rays until 5 reflections and 1 difraction.

In Fig 10 is shown the first pulses that arrives at the receiver antenna R, considering all obstacles and the ground electric perfect conductors for TD-UTD simulation. Some pulses predicted by TD-UTD are inverted when compared with those obtained by UTD-IFFT. This pulses are those reflected in ground, and the cause is that the approach of the ground as a perfect conductor it is not good enough. As the antennas heights are small when compared with the distance between them, the ray that reflect in ground has a grazing incidence, and for vertical polarization, the approach of the ground as a magnetic

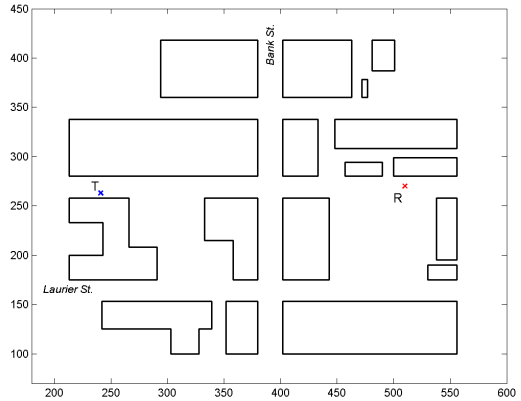

Fig. 8. Region of Ottawa city, in which the receiver is in the line of sight of the transmitter. The transmitter antenna T is an infinitesimal electric dipole vertically polarized, and the receiver R is isotropic. All dimensions are in meters.

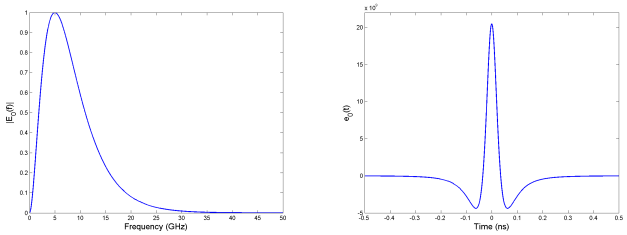

(a) Pulse spectrum. (b) Pulse in time.

Fig. 9. UWB excitation used. The pulse parameters are: $M = 1$, $N = 2$ and $f_c = 5$ GHz.

perfect conductor is the right one. Using this approach, the results shown in Fig. 11 were obtained. Now the pulses are not inverted, but they still have a difference in amplitude due to the TD-UTD not consider the losses in reflection and diffraction phenomena. The responses have a correlation coefficient of 0.967, that is a good result.

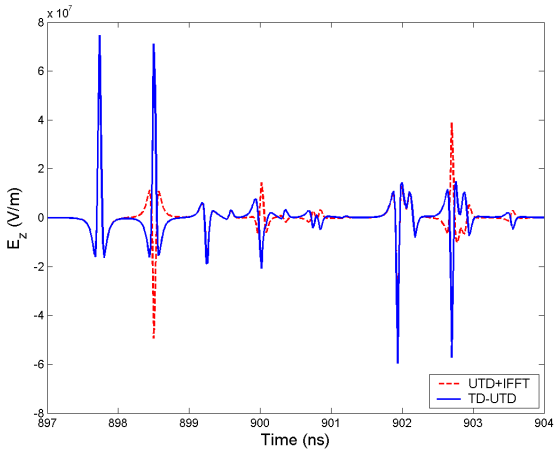

Fig. 10. Comparison between UTD-IFFT and TD-UTD in channel radio response. For TD-UTD, the obstacles and the ground were considered perfect electric conductors.

IV. Conclusions

Despite not considerate the losses, the Time Domain Uniform Theory of Diffraction (TD-UTD) is a good tool for field scattering prediction of UWB signals in urban environment whether the ground is considered as a perfect magnetic conductor and the obstacles as perfect electric conductors in the cases of vertically polarized antennas. When, for a single ray, the number of reflections increases, the difference between the UTD-IFFT and TD-UTD results becomes greater because the TD-UTD does not consider the attenuation causes by losses in obstacles and ground.

Acknowledgment

The authors wish to thank Daniela N. Schettino for her help with the ray-tracing software.

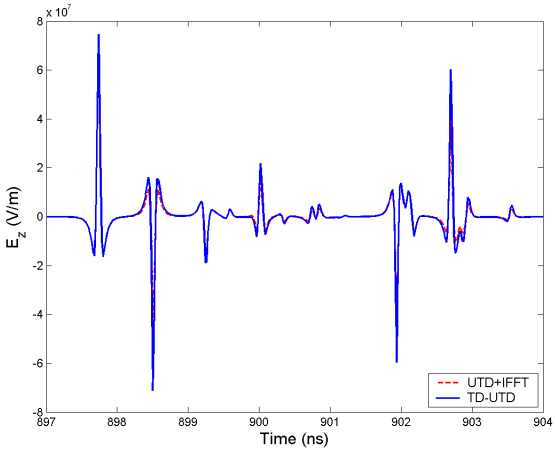

Fig. 11. Comparison between UTD-IFFT and TD-UTD in channel radio response. For TD-UTD, the obstacles were considered perfect electric conductor and the ground perfect magnetic conductor.

References

[1] K. Siwiak, "Ultra-wideband radio: A new pan and postioning technology," *IEEE Vehicular Technology Society News*, pp. 4–9, Fevereiro 2002.

[2] W. H. Press, S. A. Teukolsky, W. T. Vetterling, and B. P. Flannery, *Numerical Recipes in C*, Cambridge, Ed. Cambridge University Press, 2002.

[3] R. N. Bracewell, *The Fourier Transform and its Applications*, 2nd ed., M. Hill, Ed. New York: McGraw Hill, 1986.

[4] P. R. Rousseau and P. H. Pathak, "Time domain version of the uniform geometrical theory of diffraction," The Ohio State University, Technical Report 721564-3, Tech. Rep., Fevereiro 1996.

[5] D. A. McNamara, C. W. I. Pistorius, and J. A. G. Malherbe, *Introduction to The Uniform Geometrical Theory of Diffraction*, U. of Pretoria, Ed. Artech House, 1990.

[6] D. N. Schettino, "Técnicas assintóticas para predição de cobertura radioelétrica," Master's thesis, PPGEE/UFMG, 2002.

[7] S. Y. Tan and H. S. Tan, "A microcellular communications model based on the uniform theory of diffraction and multiple image theory," *IEEE Trans. Antennas Propagat.*, vol. 44, pp. 1317–1326, Oct. 1996.

[8] P. D. Holm, "A new heuristic utd diffraction coefficient for nonperfectly conducting wedges," *IEEE Trans. Antennas Propagat.*, vol. 48, no. 8, pp. 1211–1219, Agosto 2000.

[9] R. F. Harrington, *Field Computation by Moment Methods*, Piscataway, Ed. IEEE Press, 1993.

[10] S. Y. Tan and H. S. Tan, "Propagation model for microcellular communications applied to path loss measurements in ottawa city streets," *IEEE Trans. Veh. Technol.*, vol. 44, no. 2, pp. 313–317, Maio 1995.